Yue Bing Zheng
e-mail: yzz113@psu.edu

Bala Krishna Juluri
e-mail: bxj139@psu.edu

Brian Kiraly
e-mail: btk5051@psu.edu

Tony Jun Huang
e-mail: junhuang@psu.edu

Department of Engineering Science and Mechanics,
The Pennsylvania State University,
University Park, PA 16802

Ordered Au Nanodisk and Nanohole Arrays: Fabrication and Applications

We have utilized nanosphere lithography (NSL) to fabricate ordered Au nanodisk and nanohole arrays on substrates and have studied the localized surface plasmon resonance (LSPR) of the arrays. Through these investigations, we demonstrate that the angle-dependent behavior of the LSPR in the Au nanodisk arrays enables real-time observation of exciton-plasmon couplings. In addition, we show that the NSL-fabricated Au nanohole arrays can be applied as templates for patterning micro-/nanoparticles under capillary force. The unique structural and plasmonic characteristics of the Au nanodisk and nanohole arrays, as well as the low-cost and high-throughput NSL-based nanofabrication technique, render these arrays excellent platforms for numerous engineering applications. [DOI: 10.1115/1.4002221]

1 Introduction

Ordered metal nanostructure arrays with spatial coherence are useful for many applications in the fields of engineering and medicine [1,2]. The development of cost-effective methods to fabricate such nanostructures presents a significant challenge to the nanoscience and nanotechnology community. Although there are several nanofabrication techniques available, such as photolithography, electron beam lithography, and focused ion beam lithography, these conventional techniques are limited by their high cost, low throughput, and difficulty in accessing the facilities [3–5]. The limitations of conventional techniques have motivated the development of "unconventional" approaches, such as soft lithography, nanoimprinting lithography (NIL), and nanosphere lithography (NSL) [6–8]. In this article, we demonstrate that NSL can be used to produce ordered Au nanodisk and nanohole arrays on substrates at high throughput and low cost. NSL also allows for well-controlled morphology and size distribution of the Au nanodisks and nanoholes. These low-cost, high-throughput, and highly ordered Au nanodisks and nanoholes can be of great interest for applications, such as nanoscale waveguides, surface enhanced Raman spectroscopy, biosensors, nanopatterning, and molecular plasmonics [9,10].

In the fields of nanophotonics and plasmonics, understanding and controlling the optical behavior of molecules near the vicinity of noble metal nanoparticles is not only fundamentally important but also essential for applications, such as energy harvesting [11], nanoscale optical circuits [12], and ultrasensitive chemical and biological sensors [13,14]. Of particular interest is the recent discovery of mixed exciton-plasmon states in metal-molecule complexes where excitons of molecules resonate with the plasmon modes of metal nanoparticles. This leads to the appearance of new peaks, so-called hybridized states, in the extinction spectra [15,16]. The resonant coupling strength varies with spectral overlap between the localized surface plasmon resonance (LSPR) response and molecular resonance, therefore, a platform with tunable LSPR is essential for understanding and harvesting the mixed exciton-plasmon states. Wurtz et al. [15] demonstrated tunable exciton-plasmon coupling in J-aggregate hybridized Au nanorods by varying the thickness of air shells that surround the nanorods. Fofang et al. [16] used the highly tunable LSPR observed in Au nanoshells to understand plasmon–exciton coupling as a function of spectral overlap. Although these studies demonstrated the use of tunable LSPR to vary plasmon-exciton coupling, they required the fabrication of a large number of different nanoparticle arrays to establish exciton-plasmon hybridization. Such a large number of samples complicated the experimental procedures and introduced deviations. Here, we use coupled dipole approximations (CDA) calculations to demonstrate that the nanodisk arrays exhibit angle-dependent LSPR due to the coupling effects among the nanodisks. We also demonstrate that the angular dependence of the LSPR makes NSL-fabricated nanodisk arrays a versatile platform for better understanding plasmon-exciton couplings in real time.

In nanopatterning applications, the ability to arrange cells and micro-/nanoparticles into desired templates is critical for numerous biological applications, such as microarrays, tissue engineering, and regenerative medicine [17]. Researchers have developed a variety of particle-patterning and particle-manipulating techniques, such as microcontact printing, optical tweezers, optoelectronic tweezers, acoustic tweezers, magnetic tweezers, and electrophoresis [17–24]. Herein, we demonstrate that the NSL-fabricated Au nanohole arrays can work as effective templates for patterning micro-/nanoparticles at low cost and high throughput.

2 Theory

To overcome the limitations of the existing research on nanoparticle array-based plasmon-exciton couplings, we have used the NSL-fabricated nanodisk arrays to observe the formation of exciton-plasmon states in real time. In these investigations, we aim to achieve in situ dynamic control of the coupling strength in a single Au nanodisk array coated with J-aggregate molecules by making use of angle-dependent LSPR. To simulate the angle-resolved extinction spectra for both the bare Au nanodisk array and the array of nanodisk-J-aggregate complexes, we performed CDA calculations. In CDA, the nanoparticle array is described by an array of M dipoles, each with the dipole moment $\mathbf{P}_j = \alpha_j \mathbf{E}_j$, here α_j is the dipolar polarizability and $\mathbf{E}_j$ is the sum of the incident electric field ($\mathbf{E}_{(\mathrm{inc},j)} = \mathbf{E}_0 e^{ikr_j}$) and the electric field arising from the other M-1 dipoles ($\Sigma_{l \neq j}^{M} A_{jl} \cdot \mathbf{P}$). Thus, the total electric field on the jth dipole is given by [25]

$$\alpha_j^{-1} \mathbf{P}_j = \mathbf{E}_j = \mathbf{E}_{\mathrm{inc},j} - \sum_{l \neq j}^{M} A_{jl} \cdot \mathbf{P}_l \tag{1}$$

where the electric field from the other M-1 dipoles is given by

Manuscript received June 24, 2010; final manuscript received July 8, 2010; published online August 23, 2010. Assoc. Editor: Vijay K. Varadan.

$$A_{jl}\cdot \mathbf{P}_l = \frac{e^{ikr_{jl}}}{r_{jl}^3}\left[k^2 r_{jl}\times(r_{jl}\times P_l)+\frac{1-ikr_{jl}}{r_{jl}^2}\{r_{jl}^2\mathbf{P}_l-3r_{jl}(r_{jl}\cdot P_l)\}\right] \tag{2}$$

Dipole moment vectors for each dipole were calculated by solving the 3M complex linear equations resulting from Eqs. (1) and (2). These calculated dipole moments and incident electric fields were then used to calculate the extinction cross section of the nanoparticle based on the optical theorem [26]

$$C_{\text{ext}}(\lambda) = \frac{4\pi k}{|\mathbf{E}_0|^2}\sum_{l=1}^{M}\text{Im}(E_{\text{inc},l}^{*}\cdot \mathbf{P}_l) \tag{3}$$

where $E_{\text{inc},l}^{*}$ is the complex conjugate of $E_{\text{inc},l}$ and $k=2\pi m/\lambda$ is the wave vector. Here, m is the refractive index of the surrounding medium and λ is the free-space wavelength of the incident light. The extinction cross section is further normalized as the extinction efficiency, $Q_{\text{ext}}=C_{\text{ext}}(\lambda)/C_{\text{geom}}$, where C_{geom} is the particle's cross-sectional area projected onto a plane perpendicular to the incident beam.

To describe the polarizability of the Au nanodisk, we approximate the nanodisk by an oblate spheroid for which the in-plane polarizability is given as

$$\alpha_j = \frac{v_1(\varepsilon_1-\varepsilon_m)}{\varepsilon_m+L(\varepsilon_1-\varepsilon_m)} \tag{4}$$

where v_1 is the volume of the oblate spheroid, ε_1 is the dielectric function of Au as per the Drude model, ε_m is the dielectric constant of the surrounding medium, and L is the geometrical factor of the spheroid. We approximate the J-aggregate-covered Au nanodisk by a core oblate spheroid of Au covered with a shell layer of resonant molecules. The core-shell oblate spheroid has a polarizability given by [26]

$$\alpha_j = \frac{v_2\{(\varepsilon_2-\varepsilon_m)(\varepsilon_2+(\varepsilon_1-\varepsilon_2)(L^{(1)}-fL^{(2)}))+f\varepsilon_2(\varepsilon_1-\varepsilon_2)\}}{(\varepsilon_2+(\varepsilon_1-\varepsilon_2)(L^{(1)}-fL^{(2)}))(\varepsilon_m+(\varepsilon_2-\varepsilon_m)L^{(2)})+fL^{(2)}\varepsilon_2(\varepsilon_1-\varepsilon_2)} \tag{5}$$

where v_2 is the total volume of the core-shell oblate spheroid, f is the volume fraction of the shell layer, $L^{(1)}$ and $L^{(2)}$ are the geometrical factors of the core and core-shell spheroids, respectively, and ε_2 is the frequency-dependent dielectric function of the shell layer of resonant molecules. ε_2, expressed as $\varepsilon_2(\omega)$ to indicate the frequency dependence, is given by the Clausius–Mossotti relation [27]

$$\varepsilon_2(\omega) = \frac{3\varepsilon_o+2N\alpha_m(\omega)}{3\varepsilon_o-N\alpha_m(\omega)} \tag{6}$$

where N is the number density of the molecules, ε_o is the vacuum permittivity, $\alpha_m(\omega)$ is the frequency-dependent molecular polarizability, and ω is the angular frequency of the incident light. The molecular polarizability is given by a one-oscillator Lorentz model

$$\alpha_m(\omega) = \frac{\alpha_0\omega_o^{\,2}}{\omega_o^{\,2}-\omega^2-i\omega\Gamma} \tag{7}$$

where α_0 is the static polarizability, ω_o is the resonant angular frequency of the molecules, and Γ is the inverse of the effective excited state lifetime.

In our simulations, the Au nanodisk array was modeled as a hexagonally arranged Au oblate spheroid array with a total spheroid number M of 492, which is large enough to ensure converged results. The array had a period of 320 nm. The minor axis of the spheroid was assumed to be 17 nm while the major axis was changed between 100 nm and 125 nm so as to simulate the same wavelength range found in the experiments. The entire spheroid array was assumed to be embedded in homogeneous surroundings with $\varepsilon_m=1.562$. The value of ε_m was estimated from the averaged dielectric constant of air and glass ($\varepsilon_m=1$ and $\varepsilon_m=2.124$ for air and glass, respectively), considering that each Au nanodisk in the experiment was immobilized on a glass substrate with the upper half of the disk exposed to air. The parameters in the Lorentz model used to describe the dye molecule were chosen to match the experimental absorption spectrum of the J-aggregates, i.e., $\omega_o=1.76$ eV, $N\alpha_0=3\times10^{-14}$, and $\Gamma=0.01$ eV. To reflect the natural probe light used in the experiments, we averaged the extinction spectra over both p-polarized and s-polarized source light in the simulations.

3 Results and Discussion

Figure 1(*a*) shows a schematic of the fabrication procedure for ordered Au nanodisk arrays. First, an Au thin film of controlled thickness (~33 nm) was deposited onto a glass substrate. Second, a self-assembled monolayer (SAM) of close-packed, monodispersed polystyrene (PS) nanospheres (Duke Scientific, Palo Alto, CA) was deposited onto the Au surface [28]. Third, O_2 reactive ion etching (RIE) and Ar RIE were carried out to morph the closely packed PS nanosphere monolayer into arrays of separated nanoellipses and to selectively etch the portion of the Au film that was not protected by the nanoellipses. Removal of the PS residues with toluene left the Au nanodisks on the substrates.

The procedure for fabricating nanohole arrays in Au thin films is given in Fig. 1(*b*). A SAM of PS nanospheres was formed on a substrate, followed by O_2 RIE to tune the sphere size [29]. Au thin film of controlled thickness was deposited on the substrate with

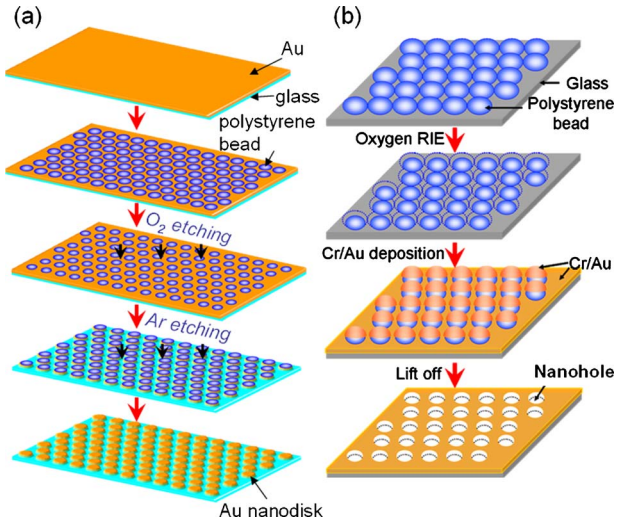

Fig. 1 (*a*) **Fabrication procedure for ordered Au nanodisk arrays and** (*b*) **fabrication procedure for ordered Au nanohole arrays**

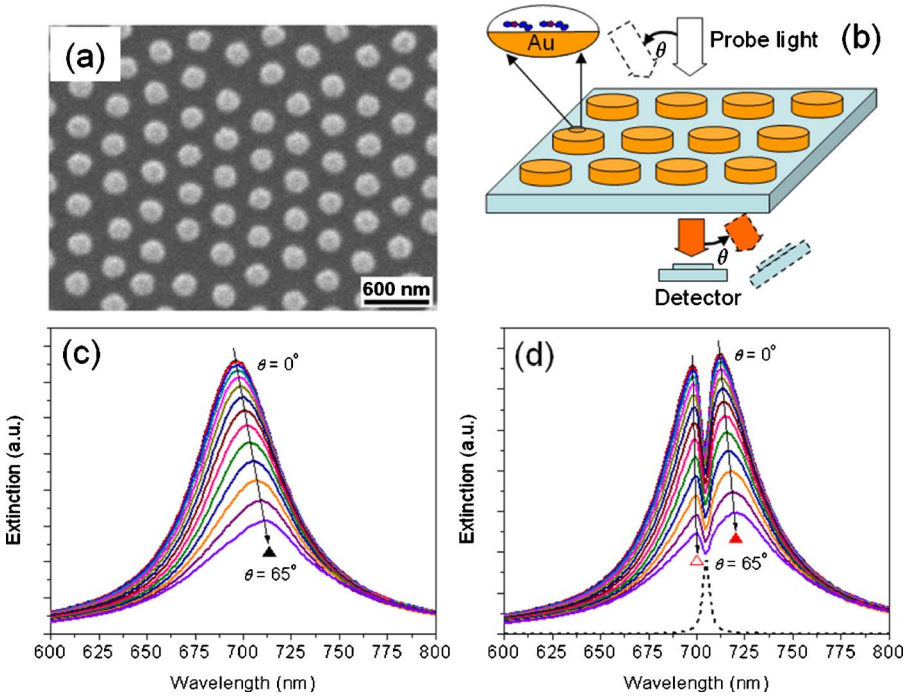

Fig. 2 (*a*) A SEM image of Au nanodisk array, (*b*) schematic of measuring angle-dependent spectra, (*c*) angle-dependent spectra of bare Au nanodisk array, and (*d*) angle-dependent spectra of array of nanodisk-J-aggregate complexes. The dashed line curve is the extinction spectrum of J-aggregates.

the etched PS spheres acting as a mask. After removal of the PS spheres via toluene/sonication, an Au thin film with highly ordered nanohole arrays was formed on the substrate.

Figure 2(*a*) shows a scanning electron microscopy (SEM) image of a hexagonally arranged Au nanodisk array on a glass substrate fabricated by NSL. The array's period was 320 nm as determined from the SEM images, which was consistent with the original diameter of PS nanospheres. The corresponding experimental setup that would be used to investigate the plasmon-exciton resonant coupling in arrays of nanodisk-J-aggregate complexes is given in Fig. 2(*b*).

Figure 2(*c*) shows the results of the angle-resolved extinction spectra simulations from a bare Au nanodisk array. We can see that the strong in-plane LSPR from the array made a continuous redshift as the incident angle was changed from 0 deg to 65 deg. The angle-resolved extinction spectra simulations for an array of the nanodisk-J-aggregate complexes are shown in Fig. 2(*d*). The strong in-plane dipole resonance of the bare Au nanodisk array splits into two bands on adsorption of J-aggregates on the disk surfaces, reflecting the resonant coupling between plasmons and excitons. Similar to the bare nanodisks, we observe that the two peaks continuously redshift as the incident angle is changed from 0 deg to 65 deg. The hybridization of plasmon resonance and molecular resonance is more obvious when the dispersion curves of the split LSPR peaks are plotted as a function of the LSPR peak of the bare nanodisks obtained at the different incident angles. Thus, by varying the angle of incident light, it is possible to explore the complete energy range necessary for examining the plasmon-exciton hybridization by using a very small number (e.g., one or two) of samples.

Next, we examine the patterning of nano-/microparticles with nanohole arrays as templates. Figure 3(*a*) shows the patterning mechanism with Au nanohole arrays as templates; in this figure, the capillary forces, which drag and confine the particles into the Au nanoholes, are illustrated. In the capillary-force-based assembly process, a certain volume of PS nanoparticle suspension is moved over the nanohole array by sliding a glass cover over the substrate. PS nanoparticles are assembled from the three-phase contact line of the receding meniscus.

As shown in Fig. 3(*a*), the capillary force F_c is exerted on the nanoparticles protruding through the liquid-air interface at a certain angle. When the meniscus moves over the flat regions of the substrate, the horizontal component of F_c on the particles dominates and pushes the particles toward the suspension, avoiding the nonspecific adsorption on the flat region of the substrate. The meniscus is deformed to have the vertical component of F_c on the particles dominant when approaching a hole. The vertical compo-

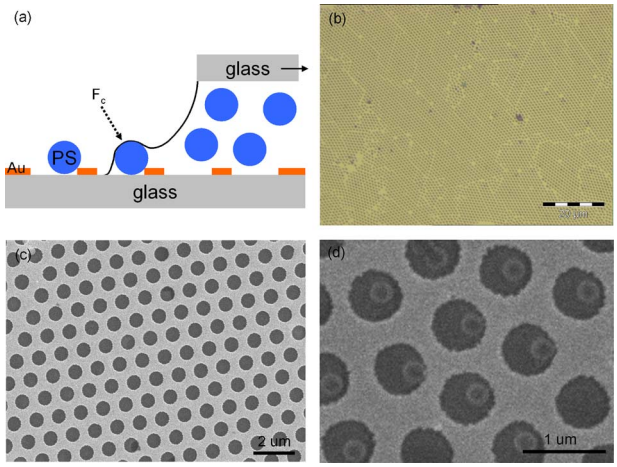

Fig. 3 (*a*) Schematic of working mechanism of patterning of particles on Au nanohole array, (*b*) an optical microscopy image of Au nanohole array, (*c*) a SEM image of Au nanohole array, and (*d*) a SEM image showing the particles confined in the holes

nent can be strong enough to push the particles into the template holes. The maximum number of particles in each hole depends on the sizes of the holes and the particles as well as the concentration of particle suspension. Figures 3(*b*) and 3(*c*) are the representative optical microscopy and SEM images of the Au nanohole arrays used as patterning templates. In these experiments, the original PS spheres of a diameter of 1 μm were used. The RIE was carried out for 8 min in O_2 gas at 20 sccm, 15 mTorr, and a power density of 100 W. Figure 3(*d*) shows an SEM image of PS nanoparticles of diameter 320 nm trapped inside the nanoholes.

4 Conclusion

In summary, we have successfully fabricated highly ordered Au nanodisk and nanohole arrays on substrates using the NSL nanofabrication method. We demonstrate that the NSL-fabricated nanodisk arrays exhibit angle-dependent LSPR properties and that the angular dependence of the LSPR makes these nanodisk arrays efficient, versatile platforms for better studying the plasmon-exciton couplings in real time. We have also demonstrated micro-/nanoparticle patterning based on the NSL-fabricated nanohole arrays. We believe that with their significant advantages in cost, simplicity, throughput, and performance, the NSL-fabricated nanodisk and nanohole arrays will find applications in fields, such as plasmonics, nanophotonics, micro-/nanofluidics, microarray, and cell biology [17–21,30–37].

Acknowledgment

This research was supported by the Air Force Office of Scientific Research, the National Science Foundation, the U.S. Department of Agriculture (USDA/NRI), and the Penn State Center for Nanoscale Science (MRSEC). Components of this work were conducted at the Pennsylvania State University node of the NSF-funded National Nanotechnology Infrastructure Network. Y. B. Z. recognizes the support from KAUST Scholar Award and the Founder's Prize and Grant of the American Academy of Mechanics. The authors thank Dr. Jinjie Shi, and Dr. Xiaole Mao for helpful discussions.

References

[1] Zhao, L. L., Kelly, K. L., and Schatz, G. C., 2003, "The Extinction Spectra of Silver Nanoparticle Arrays: Influence of Array Structure on Plasmon Resonance Wavelength and Width," J. Phys. Chem. B, **107**(30), pp. 7343–7350.

[2] Shao, D. B., and Chen, S. C., 2006, "Direct Patterning of Three-Dimensional Periodic Nanostructures by Surface-Plasmon-Assisted Nanolithography," Nano Lett., **6**(10), pp. 2279–2283.

[3] Maier, S. A., Brongersma, M. L., Kik, P. G., Meltzer, S., Requicha, A. A. G., and Atwater, H. A., 2001, "Plasmonics—A Route to Nanoscale Optical Devices," Adv. Mater., **13**(19), pp. 1501–1505.

[4] Choudhury, P., 1997, *Handbook of Microlithography, Micromachining, and Microfabrication*, SPIE Optical Engineering, Bellingham, WA.

[5] Smith, H. I., and Craighead, H. G., 1990, "Nanofabrication," Phys. Today, **43**(2), pp. 24–30.

[6] Xia, Y. N., and Whitesides, G. M., 1998, "Soft Lithography," Annu. Rev. Mater. Sci., **28**, pp. 153–184.

[7] Hulteen, J. C., and Vanduyne, R. P., 1995, "Nanosphere Lithography: A Materials General Fabrication Process for Periodic Particle Array Surfaces," J. Vac. Sci. Technol. A, **13**(3), pp. 1553–1558.

[8] Chou, S. Y., Krauss, P. R., and Renstrom, P. J., 1996, "Nanoimprint Lithography," J. Vac. Sci. Technol. B, **14**(6), pp. 4129–4133.

[9] Hutter, E., and Fendler, J., 2004, "Exploitation of Localized Surface Plasmon Resonance," Adv. Mater., **16**(19), pp. 1685–1706.

[10] Zheng, Y. B., Jensen, L., Yan, W., Walker, T. R., Juluri, B. K., Jensen, L., and Huang, T. J., 2009, "Chemically Tuning the Localized Surface Plasmon Resonances of Gold Nanostructure Arrays," J. Phys. Chem. C, **113**(17), pp. 7019–7024.

[11] Wang, H., Brandl, D. W., Nordlander, P., and Halas, N. J., 2007, "Plasmonic Nanostructures: Artificial Molecules," Acc. Chem. Res., **40**, pp. 53–62.

[12] Maier, S. A., Kik, P. G., Atwater, H. A., Meltzer, S., Harel, E., Koel, B. E., and Requicha, A. A. G., 2003, "Local Detection of Electromagnetic Energy Transport Below the Diffraction Limit in Metal Nanoparticle Plasmon Waveguides," Nature Mater., **2**(4), pp. 229–232.

[13] Novo, C., Funston, A. M., Pastoriza-Santos, I., Liz-Marzan, L. M., and Mulvaney, P., 2008, "Influence of the Medium Refractive Index on the Optical Properties of Single Gold Triangular Prisms on a Substrate," J. Phys. Chem. C, **112**(1), pp. 3–7.

[14] Odom, T. W., and Nehl, C. L., 2008, "How Gold Nanoparticles Have Stayed in the Light: The 3M's Principle," ACS Nano, **2**(4), pp. 612–616.

[15] Wurtz, G. A., Evans, P. R., Hendren, W., Atkinson, R., Dickson, W., Pollard, R. J., Zayats, A. V., Harrison, W., and Bower, C., 2007, "Molecular Plasmonics With Tunable Exciton-Plasmon Coupling Strength in J-Aggregate Hybridized Au Nanorod Assemblies," Nano Lett., **7**(5), pp. 1297–1303.

[16] Fofang, N. T., Park, T. H., Neumann, O., Mirin, N. A., Nordlander, P., and Halas, N. J., 2008, "Plexcitonic Nanoparticles: Plasmon-Exciton Coupling in Nanoshell-J-Aggregate Complexes," Nano Lett., **8**(10), pp. 3481–3487.

[17] Shi, J. J., Ahmed, D., Mao, X., Lin, S. C. S., Lawit, A., and Huang, T. J., 2009, "Acoustic Tweezers: Patterning Cells and Microparticles Using Standing Surface Acoustic Waves (SSAW)," Lab Chip, **9**(20), pp. 2890–2895.

[18] Shi, J. J., Huang, H., Stratton, Z., Huang, Y. P., and Huang, T. J., 2009, "Continuous Particle Separation in a Microfluidic Channel Via Standing Surface Acoustic Waves (SSAW)," Lab Chip, **9**(23), pp. 3354–3359.

[19] Mao, X., Lin, S. C. S., Dong, C., and Huang, T. J., 2009, "Single-Layer Planar on-Chip Flow Cytometer Using Microfluidic Drifting Based Three-Dimensional (3D) Hydrodynamic Focusing," Lab Chip, **9**(11), pp. 1583–1589.

[20] Shi, J. J., Mao, X., Ahmed, D., Colletti, A., and Huang, T. J., 2008, "Focusing Microparticles in a Microfluidic Channel With Standing Surface Acoustic Waves (SSAW)," Lab Chip, **8**(2), pp. 221–223.

[21] Mao, X., Waldeisen, J. R., and Huang, T. J., 2007, "Microfluidic Drifting—Implementing Three-Dimensional Hydrodynamic Focusing With a Single-Layer Planar Microfluidic Device," Lab Chip, **7**(10), pp. 1260–1262.

[22] Dufresne, E. R., and Grier, D. G., 1998, "Optical Tweezer Arrays and Optical Substrates Created With Diffractive Optics," Rev. Sci. Instrum., **69**(5), pp. 1974–1977.

[23] Righini, M., Zelenina, A. S., Girard, C., and Quidant, R., 2007, "Parallel and Selective Trapping in a Patterned Plasmonic Landscape," Nat. Phys., **3**(7), pp. 477–480.

[24] Geissler, M., and Xia, Y. N., 2004, "Patterning: Principles and Some New Developments," Adv. Mater., **16**(15), pp. 1249–1269.

[25] Purcell, E. H., and Pennypacker, C. R., 1973, "Scattering and Absorption of Light by Non-Spherical Dielectric Grains," Astrophys. J., **186**, pp. 705–714.

[26] Bohren, C. F., and Huffman, D. R., 1983, *Absorption and Scattering of Light by Small Particles*, Wiley, New York.

[27] Zheng, Y. B., Yang, Y. W., Jensen, L., Fang, L., Juluri, B. K., Flood, A. H., Weiss, P. S., Stoddart, J. F., and Huang, T. J., 2009, "Active Molecular Plasmonics: Controlling Plasmon Resonances With Molecular Switches," Nano Lett., **9**(2), pp. 819–825.

[28] Zheng, Y. B., Juluri, B. K., Mao, X., Walker, T. R., and Huang, T. J., 2008, "Systematic Investigation of Localized Surface Plasmon Resonance of Long-Range Ordered Au Nanodisk Arrays," J. Appl. Phys., **103**(1), p. 014308.

[29] Chong, M. A. S., Zheng, Y. B., Gao, H., and Tan, L. K., 2006, "Combinational Template-Assisted Fabrication of Hierarchically Ordered Nanowire Arrays on Substrates for Device Applications," Appl. Phys. Lett., **89**, p. 233104.

[30] Ahmed, D., Mao, X., Juluri, B. K., and Huang, T. J., 2009, "A Fast Microfluidic Mixer Based on Acoustically Driven Sidewall-Trapped Microbubbles," Microfluid. Nanofluid., **7**(5), pp. 727–731.

[31] Ahmed, D., Mao, X., Shi, J. J., Juluri, B. K., and Huang, T. J., 2009, "A Millisecond Micromixer via Single-Bubble-Based Acoustic Streaming," Lab Chip, **9**(18), pp. 2738–2741.

[32] Hsiao, V. K. S., Zheng, Y. B., Juluri, B. K., and Huang, T. J., 2008, "Light-Driven Plasmonic Switches Based on Au Nanodisk Arrays and Photoresponsive Liquid Crystals," Adv. Mater., **20**(18), pp. 3528–3532.

[33] Juluri, B. K., Lu, M., Zheng, Y. B., Huang, T. J., and Jensen, L., 2009, "Coupling Between Molecular and Plasmonic Resonances: Effect of Molecular Absorbance," J. Phys. Chem. C, **113**(43), pp. 18499–18503.

[34] Juluri, B. K., Zheng, Y. B., Ahmed, D., Jensen, L., and Huang, T. J., 2008, "Effects of Geometry and Composition on Charge-Induced Plasmonic Shifts in Gold Nanoparticles," J. Phys. Chem. C, **112**(19), pp. 7309–7317.

[35] Mao, X., Juluri, B. K., Lapsley, M. I., Stratton, Z. S., and Huang, T. J., 2010, "Milliseconds Microfluidic Chaotic Bubble Mixer," Microfluid. Nanofluid., **8**(1), pp. 139–144.

[36] Mao, X., Lin, S. C. S., Lapsley, M. I., Shi, J. J., Juluri, B. K., and Huang, T. J., 2009, "Tunable Liquid Gradient Refractive Index (L-Grin) Lens With Two Degrees of Freedom," Lab Chip, **9**(14), pp. 2050–2058.

[37] Zheng, Y. B., Huang, T. J., Desai, A. Y., Wang, S. J., Tan, L. K., Gao, H., and Huan, A. C. H., 2007, "Thermal Behavior of Localized Surface Plasmon Resonance of Au/TiO_2 Core/Shell Nanoparticle Arrays," Appl. Phys. Lett., **90**(18), p. 183117.